Vietnam Journal of Catalysis and Adsorption
Tạp chí xúc tác và hấp phụ Việt Nam

https://jca.edu.vn

# Vanadium-doped $TiO_2$ Adsorbent-Photocatalyst for Organic Dye Treatment

Nguyen Thi Thom[1], Nghiem Thi Thuong[1], Hoang Huu Hiep[1], Cao Hong Ha[1], Nguyen Vân-Anh[1,*]

[1] *School of Chemistry and Life Sciences, Hanoi University of Science and Technology, Hanoi, VIETNAM*
**Email: anh.nguyenvan@hust.edu.vn*

ARTICLE INFO

Received: 03/4/2024
Accepted: 18/5/2024
Published: 30/06/2024

*Keywords:*
V doped $TiO_2$, Adsorption-Photocatalyst, Modified Polyol synthesis, MB, RhB.

ABSTRACT

This study focuses on the synthesis of V-doped $TiO_2$ materials using a modified polyol method to enhance their efficiency. The obtained materials were characterized by various methods such as XRD, EDX, FTIR, SEM, TEM-SAED, Raman, and UV-Vis DRS. The results indicated the crystalline anatase phase of $TiO_2$, with spherical morphology and an average size of 30nm. The UV-DRS measurement demonstrated that doped materials have a lower bandgap than the pristine $TiO_2$. The material possesses dual functionality, with adsorption capability and photocatalytic activity applied to treat organic dye contaminants. Evaluation of MB degradation under UV irradiation revealed an exceptional efficiency of up to 99% within a remarkably short duration of 30 minutes. Furthermore, the catalyst exhibited robust recovery efficiency exceeding 99% after 2 regeneration cycles and retention of approximately 80% after four cycles.

## 1. Introduction

Recently, water scarcity and pollution have become increasingly threatening issues to human health and the environment. Alongside development, growth, and national policies, industrial wastewater is becoming more polluted and difficult to treat [1]. Catalytic photocatalysis holds significant potential for eliminating hazardous chemicals from the environment, owing to its efficiency and wide-ranging applicability. Several semiconductor photocatalysts for pollutant degradation have been identified, with $TiO_2$ emerging as one of the most promising due to its high photocatalytic efficiency, physical and chemical stability, non-toxic nature, and safety at room temperature and pressure. $TiO_2$ materials are expected to play a crucial role in addressing many environmental challenges and severe pollution due to their excellent capability to decompose various pollutants [2].

Nevertheless, the application of $TiO_2$ faces challenges due to its wide bandgap (3.2 eV), necessitating ultraviolet (UV) radiation to activate photocatalysis ($\lambda$ < 387 nm) [3]. UV light accounts for only about 5% of solar radiation, while visible light, constituting approximately 45% of unused solar energy [4], remains largely untapped. The shift in $TiO_2$ photocatalytic reactions from UV to the visible spectrum will profoundly impact the efficiency of utilizing solar energy in such reactions [5]. Additionally, the relatively high recombination rate of electron-hole pairs in $TiO_2$ leads to low quantum yields and poor degradation efficiency in photocatalytic reactions [6]. These limitations hinder the photocatalytic degradation properties of $TiO_2$ and its full utilization of solar energy. Hence, enhancing the photocatalytic activity of $TiO_2$ under visible light irradiation is crucial [7].

In this paper, we selected vanadium (V) doping into the crystal lattice of $TiO_2$ using the polyol method to enhance the bandgap energy of $TiO_2$ for applications in the visible light region. Vanadium metal has garnered significant interest from researchers because it belongs to Group VB with an electronic configuration similar to that of Ti, which belongs to Group IVB and is adjacent

https://doi.org/10.62239/jca.2024.045

to the periodic table. Moreover, due to the ion radius of V being approximately 0.059 nm, which is close to the ion radius of Ti at 0.068 nm [8], V can readily substitute for Ti in the crystal lattice.

## 2. Experimental

### *Materials*

The chemicals used in the present study were of analytical grade. Ethylene glycol ($C_2H_4(OH)_2$), sodium acetate ($CH_3COONa$), ethanol ($C_2H_5OH$), titanium tetrachloride ($TiCl_4$), and ammonium metavanadate ($NH_4VO_3$), Vanadium (V) oxide ($V_2O_5$) were purchased from Sigma-Aldrich Co. LLC. The chemicals were used as received without further purification. Methylene blue (MB) and Rhodamine B (RhB) were purchased from Aladin, China.

### *Synthesis of V-doped $TiO_2$ catalysts*

A specified amount of $NH_4VO_3$ was dissolved into 50 mL of ethylene glycol and heated to 60°C for 30 minutes to obtain a solution (I). Concurrently, 16.2 g $CH_3COONa$ was dissolved in 50 mL ethylene glycol [9] for 30 minutes at 60°C to yield solution (II). Solution (II) was then slowly added dropwise to the solution (I) to obtain a solution (III), followed by the precise addition of $TiCl_4$ into the cooled solution (III). The resulting solution was refluxed at 160°C for 3 hours [9]. Subsequently, the obtained solution was centrifuged and washed with $C_2H_5OH$. The resulting catalyst was dried for 15 hours at 80°C, then calcined at 500°C for 4 hours, and finely ground in a mortar. Samples synthesized via the polyol method are denoted as x V-$TiO_2$ (x = $n_V$:$n_{Ti}$ =0; 0.1). 2g of 0.1 V – $TiO_2$ synthesized via the polyol method was dispersed in 120 mL of $10^{-3}$M $H_3PO_4$ for 30 minutes [10]. It was then transferred to a hydrothermal autoclave and heated at 180°C for 12 hours. The resulting sample was obtained by centrifugation, followed by several washes with distilled water to remove impurities, and dried at 80°C for 12 hours to obtain the modified V-doped $TiO_2$ product, denoted as 0.1 V - $TiO_2$ (BT).

### *Catalysts characterization*

The crystalline phase of V–doped TiO2 was investigated by X-ray diffraction (D8 Advance–Bruker, Germany) over 2θ range from 20° to 80° using CuKα (λ = 1.5406 Å) at an intensity of 40 mA and 40kV as the X-ray emission source. The presence of elements in the material was determined by the EDX spectrum (JEOL JSM–2300, Japan). The material formation was observed by FT–IR spectrum (Jasco 4600, Japan) and Raman spectrum (LabRAM HR Evol using an excitation laser with a wavelength of 532 nm and a measuring range of 100 - 1500 $cm^{-1}$). The decrease in dye concentration was recorded on a UV–Vis spectrophotometer (Hach DR 6000). The surface morphology of V–doped $TiO_2$ was observed using SEM images (Hitachi S – 4800, Japan). The distribution of V within the $TiO_2$ crystal lattice was determined by TEM-SAED images (JEM2100, JEOL–Japan). The band gap energy was recorded by UV–Vis DRS spectrum (U-4100 Hitachi, Japan).

### *Adsorption–Photocatalytic activity measurements*

An amount of 30 mg of catalyst was dispersed in 100 mL of dye solution (MB and RhB), with concentration $C_o$ = 10 mg/L. The suspension was ultrasonically vibrated for 5 min (53 KHz), followed by magnetic stirring for 30 minutes in the dark at room temperature to establish the adsorption-desorption equilibrium of the dye. Then, a UV round bulb (20 W) was set to illuminate the reaction vessel in a vertical direction for 240 min in the dark; the distance between the UV bulb and the bottom of the beaker was 180 mm. At specific intervals of every 15 minutes, 2.0 mL of the suspension was withdrawn and filtered with a 0.22 µm filter to remove the remaining catalyst in the solution. Then, the decolorization of the dye was measured using a UV-Vis spectrophotometer at the peak wavelength of MB and RhB of 664 nm and 554 nm, respectively. The degradation efficiency of V – doped $TiO_2$ (H %) was computed by using equation (1):

$$H\ (\%) = \frac{C_o - C_t}{C_o} \times 100\% \qquad (1)$$

Where H is the degradation efficiency, $C_o$ and $C_t$ are the initial concentrations and the concentrations at the time t of the dye, respectively.

## 3. Results and discussion

### *XRD analysis*

The X-ray diffraction (XRD) results in Figure 1A reveal crystalline phase changes upon the catalyst material modification with $H_3PO_4$. Specifically, in the XRD pattern of the 0.1V-$TiO_2$ (BT) sample, a characteristic diffraction peak appears at $2\theta$ = 25.325°, corresponding to the crystal face of $TiO_2$ in the anatase phase. In contrast, for the unmodified material sample, 0.1V-$TiO_2$, the characteristic diffraction peak appears at $2\theta$ = 31.68°, corresponding to the crystal face of $TiO_2$ in the brookite phase. Thus, the modification induces a transition of the material's characteristic crystal face from brookite to anatase. Additionally, other diffraction peaks are observed at $2\theta$ = 37.835°, 47.855°, and 54.005°, corresponding to the (004), (200), and (105) planes of $TiO_2$ in the anatase phase; $2\theta$ = 29.945°, 32.525°, and

https://doi.org/10.62239/jca.2024.045

58.265°, corresponding to the (121), (200), and (232) planes of $TiO_2$ in the brookite phase; and 2θ = 44.405°, corresponding to the (210) plane of $TiO_2$ in the rutile phase (compared with JCPDS 00-029-1360).

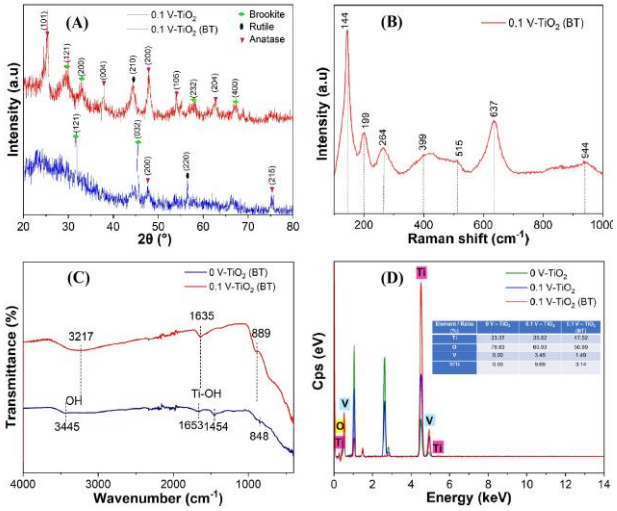


Fig. 1: (A) XRD patterns of samples 0.1 V - $TiO_2$, 0.1 V - $TiO_2$ (BT); (B) Raman spectra of sample 0.1 V - $TiO_2$ (BT); (C) FT-IR spectra of samples 0 V - $TiO_2$ (BT), 0.1 V - $TiO_2$ (BT); The EDX spectrum of samples 0 V - $TiO_2$, 0.1 V - $TiO_2$, 0.1 V - $TiO_2$ (BT).

To further confirm the successful incorporation of vanadium ions into the $TiO_2$ crystal lattice, Raman spectroscopy was performed to identify the characteristic vibrational modes of the material. The results are depicted in Figure 1B. The Raman spectrum of the 0.1 V-$TiO_2$ (BT) sample confirms the presence of the anatase $TiO_2$ crystalline phase in the composite via the appearance of characteristic peaks corresponding to the vibrational modes of anatase $TiO_2$: 144 $cm^{-1}$ ($E_g$); 199 $cm^{-1}$ ($E_g$); 399 $cm^{-1}$ ($B_{1g}$); 515 $cm^{-1}$ ($A_{1g}$ + $B_{1g}$); 637 $cm^{-1}$ (Eg) [11]. Several reports have identified vibrational peaks of vanadium at 141, 196, and 403 $cm^{-1}$ assigned to $V_2O_5$ (V-O) vibrations [12]. Notably, some vibrational peaks of anatase $TiO_2$ coincide with those of $V_2O_5$.

## *EDX analysis*

The X-ray energy dispersion (EDX) spectrum reveals the presence of Ti, O, and V elements in the material composition, as depicted in Figure 1D. Comparative analysis of elemental composition ratios in the material before and after modification (The inset table in Figure 1D) indicates that the V/Ti ratio in the 0.1 doping sample was 9.69% before modification. However, after material modification with $H_3PO_4$, the V/Ti ratio decreases to over 3%. This suggests that $H_3PO_4$ treatment has partially removed vanadium from the material surface during hydrothermal treatment, altering the elemental ratios within the material.

## *FTIR and Raman analysis*

The results of the Fourier-transform infrared (FTIR) spectroscopy presented in Figure 1C indicate variations in characteristic peaks associated with vanadium bonding in the $TiO_2$-V composite compared to the pristine $TiO_2$ sample. Peaks ranging from 3200 – 3600 $cm^{-1}$ are characteristic of symmetric and asymmetric stretching vibrations of hydroxyl groups (Ti - OH and/or adsorbed water), while those from 1100 – 1650 $cm^{-1}$ are attributed to bending vibrations of OH bonds in hydroxyl groups (Ti-OH) [13]. The presence of numerous -OH groups on the $TiO_2$ surface enhances the catalytic activity in organic compound decomposition processes [14]. Upon doping V into $TiO_2$, characteristic peaks related to $TiO_2$ vibrations are essentially retained, albeit with slight shifts in peak positions, resulting in minor wavenumber changes from 848 $cm^{-1}$ to 889 $cm^{-1}$, reflecting the presence of vanadium in the $TiO_2$ crystal lattice. Thus, FTIR spectroscopy has identified bonding configurations in the $TiO_2$-V composite material.

## *Morphological properties*

The SEM image in Figure 2B illustrates that the 0.1 V-$TiO_2$ sample exhibits a plate-like morphology, similar to the needle-like shape of brookite $TiO_2$ previously reported [15]. In contrast, the modified material 0.1 V-$TiO_2$ (BT) in Figure 2C appears more spherical, resembling the predominant morphology of $TiO_2$, particularly anatase $TiO_2$ [16]. Thus, after modification with $H_3PO_4$, there is a noticeable change in the morphological characteristics of the material compared to its unmodified state.

Table 1: Calculated crystal plane distances from SAED

| No | 1/r ($nm^{-1}$) | r (nm) | d ($A^0$) | (hkl) |
|---|---|---|---|---|
| 1 | 2.817 | 0.355 | 3.55 | **(101) – A** |
| 2 | 3.704 | 0.270 | 2.70 | (200) – B |
| 3 | 5.291 | 0.189 | 1.89 | **(200) – A** |
| 4 | 6.289 | 0.159 | 1.59 | (232) – B |
| 5 | 7.353 | 0.136 | 1.36 | (400) - B |

The internal structure of the 0.1 V – $TiO_2$ (BT) sample was investigated using transmission electron microscopy (TEM), as shown in Figure 2D. TEM results reveal that the material consists of alternating spherical particles and irregular-shaped phases: spherical particles correspond to anatase $TiO_2$ [17], while the plate-like structures represent $TiO_2$ brookite [15].

https://doi.org/10.62239/jca.2024.045

Observation of selected area electron diffraction (SAED) patterns in Figure 2E confirms that the nanoparticles exhibit a polycrystalline structure of anatase $TiO_2$ [16]. At the same time, the aligned nanorods present a single-crystalline structure of brookite $TiO_2$ [15] From the SAED results, the interplanar distances corresponding to the diffraction rings can be calculated, as shown in Table 1. By comparing these results with previous findings, it can be inferred that the crystal planes present in the material structure calculated from SAED are consistent with XRD and Raman spectroscopy results.

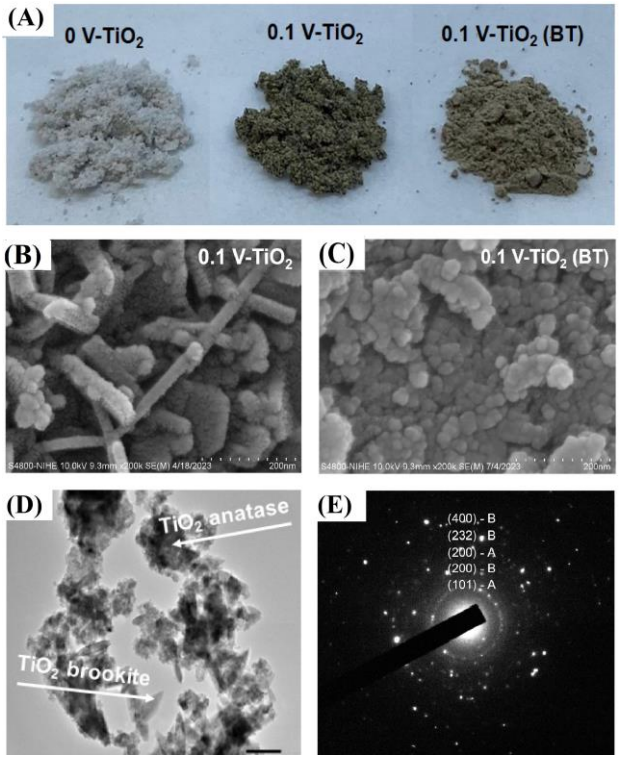


Fig. 2: (A) Experimental samples; (B) SEM images of the 0.1 V – $TiO_2$; (C) SEM images, (D) TEM image, and (E) SAED image of the 0.1 V-$TiO_2$ (BT) sample

### *UV – Vis diffuse reflectance spectroscopy (DRS)*

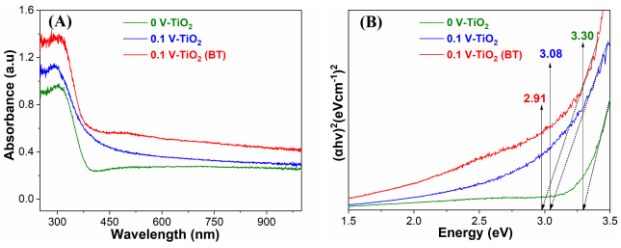


Fig. 3: (A) UV-vis DRS spectrum; (B) Bandgap energy plot according to the Tauc equation for undoped, unmodified, and 0.1 V doped samples

The UV-Vis DRS spectrum is depicted in Figure 3A, and the bandgap energy of the material is determined based on the Tauc equation (Figure 3B). Doping the material with 0.1 V using $H_3PO_4$ resulted in a decrease in the bandgap energy from 3.08 eV to 2.91 eV. This can be explained by doping the sample with $H_3PO_4$ led to the partial removal of V, causing a reduction in the bandgap energy. Consequently, the introduction of V into $TiO_2$ resulted in a decrease in the bandgap energy from 3.30 eV to 3.08 eV, and further modification of the material resulted in a bandgap energy of only 2.91 eV.

### *Adsorption equilibrium*

Conduct an investigation into the adsorption of 0.1 V – $TiO_2$ (BT) material on a solution containing MB dye with a concentration of $10^{-5}$M, equivalent to 3.2 mg/L, as depicted in Figure 4A. A comparison with the referenced work by Kwang Sun Ryu [18] (which achieved 20% removal after 5 minutes and 82% removal after 60 minutes) reveals that the 0.1 V–$TiO_2$ (BT) material exhibits significantly higher efficiency (achieving 85% removal after 5 minutes and 95% removal after 60 minutes).

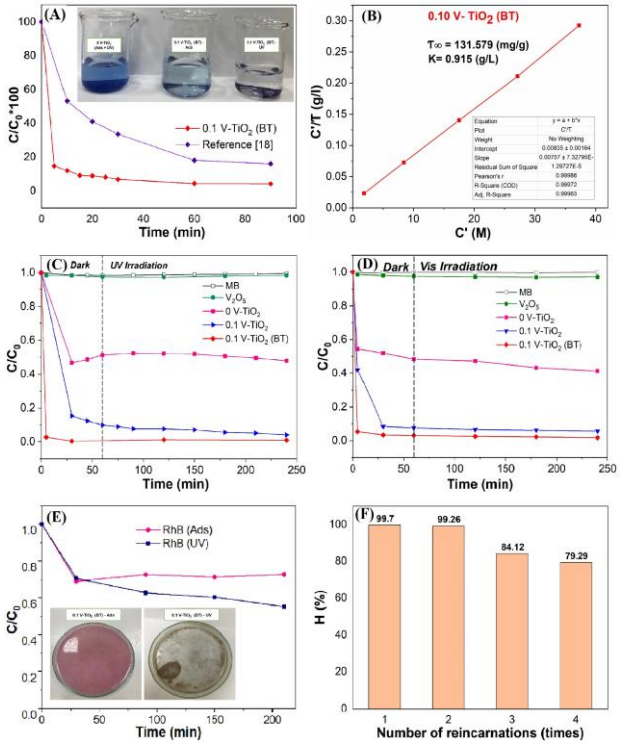


Fig. 4: (A) Graph of $C/C_0$ – t, (B) Graph of C' – C'/Γ investigating the adsorption of MB over time of 0.1 V – $TiO_2$ (BT) samples; (C) & (D) MB treatment efficiency of 0.1 V – $TiO_2$ and 0.1 V – $TiO_2$ (BT) samples under UV and Visible light, respectively; (E) RhB treatment efficiency of 0.1 V – $TiO_2$ (BT) sample; (F) Investigation of the regenerative capability of 0.1 V-$TiO_2$ (BT) material

The MB decolorization process can be divided into three adsorption stages: (i) immediate adsorption of MB within 5 minutes, (ii) gradual attainment of equilibrium

state from 5 to 60 minutes, and (iii) establishment of equilibrium state of MB molecules on 0.1 V – $TiO_2$ (BT) after 60 minutes. The results in Figure 4B depict the relationship between concentration and adsorption capacity obtained with an $R^2$ = 0.99972 (> 0.99). It can be concluded that the material follows the Langmuir equation [19] with K = 0.915 (g/L); $\Gamma_\infty$ = 131.6 (mg/g).

*Photocatalytic -adsorptive activity*

Figure 4 presents the treatment of MB and RhB using the synthesized materials. A comparison of the photocatalytic treatment efficiency of MB, $V_2O_5$, and V–$TiO_2$ modified and unmodified samples is presented in Figure 4C.

After 30 minutes of adsorption, the $V_2O_5$ sample achieved 3%, the pure V sample reached 55%, the 0.1% V-$TiO_2$ sample achieved 85%, and the 0.1% V-$TiO_2$ (BT) sample nearly reached 100%. From the experiment, it can be inferred that the material exhibits dual functionality: adsorption-photocatalysis. The adsorption efficiency reaches nearly 100% after 30 minutes, opening up a new intriguing discovery in the field of industrial wastewater treatment, where large volumes of wastewater can be initially processed through adsorption, followed by catalyst reuse via UV and visible light photocatalytic treatment (Figure 4 C and D).

For further understanding of the photocatalytic-adsorption nature of the 0.1 V–$TiO_2$ (BT) material, experiments were conducted with RhB. Comparing the efficiency of RhB treatment showed higher effectiveness when using UV in addition to adsorption alone.

Samples subjected to 30 minutes of adsorption were exposed to UV for four days, revealing that after sufficient UV exposure, the pink color of RhB had been treated, and the catalyst was regenerated, as demonstrated in Figure 4E. Table 2 compares the efficiency of treating MB by the synthesized material samples with several reported materials. With the same amount of the catalyst, the MB treatment efficiency presented in this report is several times higher, indicating the potential application of this catalyst material in treating organic pollutants.

Table 2: Comparison of photocatalytic activities of various material samples

| Sample/method | $S_{BET}$ ($m^2/g$) | Reaction conditions | Efficiency/time | Ref. |
|---|---|---|---|---|
| $TiO_2$ | 158 | 10 mg sample dispersed in 250mL MB | 40%/5min | [20] |
| 0.01 V-$TiO_2$ / Sol-gel | 152 | 0.026 mg $L^{-1}$ | 92%/5min | |
| 0.05 V-$TiO_2$ / Sol-gel | 16.5 | 100 mg sample dispersed in 300 mL MB 20 mg $L^{-1}$ | 25%/1h; 90%/8h | [21] |
| 0.1 V-$TiO_2$ / Sol-gel | 73.92 | 10 mg sample dispersed in 100mL MB 3.2 mg $L^{-1}$ | 85.2%/2h | [22] |
| 0.1 V-$TiO_2$ (BT) / Modified polyol | 132.92 | 30 mg sample dispersed in 100mL MB 10 mg $L^{-1}$ | 98%/5min | This study |

*Catalyst recycle*

The 0.1 V-$TiO_2$ (BT) material was employed to investigate its regeneration capability in the degradation of MB with a concentration of 10 mg/L over 120 minutes, followed by recovery through room-temperature washing and drying. The regenerated catalyst material was then reused for subsequent reaction runs. The results of the regeneration capability assessment are depicted in Figure 4F. After two regeneration cycles, the MB decolorization efficiency of the catalyst remained high (above 99%). However, in the third and fourth regeneration cycles, treatment efficiency decreased by approximately 15% and 5% compared to the previous cycles. This could be attributed to the aging of active sites on the catalyst surface after each reaction cycle and affecting its participation in subsequent reaction processes.

## 4. Conclusion

In this paper, we have successfully synthesized vanadium-doped $TiO_2$ materials using the polyol modification method, with the best investigation ratio achieved at nV:nTi = 0.1. Comparing the 0.1 V-$TiO_2$ (BT) photocatalyst to the undoped sample (3.30 eV) and unmodified sample (3.08 eV), the latter two showed a wider bandgap (2.91 eV). The V-doped $TiO_2$ material demonstrates dual functionality: adsorption-photocatalysis and has been tested on MB, achieving a treatment efficiency of approximately 99% after 30 minutes. Langmuir isotherm description appropriately characterizes the adsorption equilibrium. The reusability efficiency reaches nearly 80% after four regeneration cycles. V-doped $TiO_2$ material synthesized via the polyol modification method exhibits high efficiency, good

https://doi.org/10.62239/jca.2024.045

regeneration, and applicability in processing large quantities of organic dye. In future experiments, adjusting synthesis conditions may yield materials with significantly enhanced photocatalytic activity, lowering the bandgap energy for application in visible light regions.

## Acknowledgments

This work was funded by the Vietnam Ministry of Education and Training (MOET) under the Grant CT 2022.04.BKA.02.

## References

1. M. Anpo, S. Dohshi, M. Kitano, Y. Hu, M. Takeuchi, M. Matsuoke, Annu. Rev. Mater. Res. 35 (2005) 1-27. https://doi.org/10.1146/annurev.matsci.35.100303.121340
2. X. Li, F. Li, C. Yang, W. Ge, J. Photochem. Photobiol. A Chem. 141 (2001) 209-217. https://dx.doi.org/10.1016/S1010-6030(01)00446-4
3. C. Burda, Y. Lou, X. Chen, A.C.S. Samia, J. Stout, J. Gole, Nano Lett. 3 (2003) 1049-1051. https://doi.org/10.1021/nl034332o
4. S. Yin, H. Yamaki, M. Komatsu, Q. Zhang, J. Wang, Q. Tang, F. Saito, T. Sato, J. Mater. Chem. 13 (2003) 2996.
5. H. Irie, Y. Wanatabe, K. Hashimoto, J. Phys. Chem. B 107 (2003) 5483-5486. https://dx.doi.org/10.1021/jp030133h
6. Chen, X., Mao, S.S., Chem. Rev. 38 (41) (2007) 2891–2959.
7. Cui, X., Li, Y., Zhang, Q., Int. J. Photogr. 1110–662X (2012) 1302–1312.
8. J. C. S. Wu and C. H. Chen, J Photochem Photobiol A Chem 163 3 (2004). https:// 10.1016/j.jphotochem.2004.02.007.
9. K. Belfaa, M. S. Lassoued, S. Ammar, and A. Gadri, Journal of Materials Science: Materials in Electronics 29 12 (2018), https://10.1007/s10854-018-9080-6.
10. G. Zerjav, K. Zizek, J. Zavasnik, and A. Pintar, J Environ Chem Eng 10 3 (2022) 107722. https:// 10.1016/j.jece.2022.107722.
11. S. Stojadinoviyc, N. Radi, P. Stefanov, Z. Dohcevic-Mitrovic d, B. Grbic, R. Vasilc, Materials Chemistry and Physics. 151 (2015) 337-44. https://doi.org/10.1016/j.matchemphys.2014.11.077
12. B. W. Mwakikunga, M. Maaza, K. T. Hillie, C. J. Arendse, T. Malwela, and E. Sideras-Haddad, Vib Spectrosc 61 (2012). https://10.1016/j.vibspec.2012.02.007.
13. T. Dao Thi, L. Phung Thi, M. Nguyen Thi, H. Nguyen Ngoc, H. Nguyen Thi Thu, and C. Le Minh, Vietnam Journal of Catalysis and Adsorption 10 3 (2021) 113-120. https://s10.51316/jca.2021.059.
14. Y. Wu, J. Zhang, L. Xiao, and F. Chen, Appl Surf Sci 256 13, (2010) 4260-4268. https://10.1016/j.apsusc.2010.02.012.
15. T. A. Kandiel, L. Robben, A. Alkaim, and D. Bahnemann, Photochemical and Photobiological Sciences 12 (2013) 602-209. https://10.1039/c2pp25217a.
16. W. Avansi, R. Arenal, V. R. De Mendonça, C. Ribeiro, and E. Longo, CrystEngComm 16 23 (2014) 5021-5027. https://10.1039/c3ce42356e.
17. S. Dai, Y. Wu, T. Sakai, Z. Du, H. Sakai, and M. Abe, Nanoscale Res Lett 5 11 (2010) 1829-1835. https://10.1007/s11671-010-9720-0.
18. T. B. Nguyen, M. J. Hwang, and K. S. Ryu, Appl Surf Sci 258 19 (2012) 7299-7305. https://10.1016/j.apsusc.2012.03.148.
19. J. Zhang, Y. Li, L. Li, W. Li, and C. Yang, ACS Sustain Chem Eng 6 10 (2018) 12893-12905. https://10.1021/acssuschemeng.8b02264.
20. Khan, H., Berk, D., Journal of Sol-Gel Science and Technology 68(2) (2013). https://10.1007/s10971-013-3150-2.
21. Lin, W. C., Lin, Y. J., Environmental Engineering Science, 29(6) (2012). https://10.1089/ees.2010.0350.
22. Nguyen, T. B., Hwang, M. J., & Ryu, K. S., Applied Surface Science 258(19) (2012). https// 10.1016/j.apsusc.2012.03.148.